MULTIPLE TIME SCALE NUMERICAL METHODS FOR THE INVERTED PENDULUM PROBLEM

RICHARD SHARP, YEN-HSI TSAI, AND BJORN ENGQUIST

ABSTRACT. In this article, we study a class of numerical ODE schemes that use time filtering strategy and operate in two time scales. The algorithms follow the framework of the heterogeneous multiscale methods (HMM) [1]. We apply the methods to compute the averaged path of the inverted pendulum under a highly oscillatory vertical forcing on the pivot. The averaged equation for the related problems has been studied analytically in [9]. We prove and show numerically that the proposed methods approximate the averaged equation and thus compute the average path of the inverted pendulum.

1. INTRODUCTION

The central focus of this paper is the application of numerical methods for dynamical systems whose solutions oscillate around a slow manifold. We assume that the oscillations take place on a much faster time scale than the rate of change of the slow manifold with respect to time. More precisely, we hypothesize that the wavelength of the fast oscillations is proportional to a positive constant ε, and that in an $O(\varepsilon)$ time interval the slow manifold changes by at most $O(\varepsilon)$. This is the case in the inverted pendulum problem with highly oscillatory forcing, and we will show that our methods yield consistent approximations to the averaged equations.

We consider the inverted pendulum example, in which the pivot of a rigid pendulum with length l is attached to a strong periodic forcing, vibrating vertically with wavelength $2\pi\varepsilon$ and amplitude $C\varepsilon^{-1}$. The system has one degree of freedom, and can be described by the angle, θ, between the pendulum arm and the upward vertical direction, as shown in Figure 1.1. The motion is determined by

$$l\ddot{\theta} = (g + \frac{1}{\varepsilon}\sin(2\pi\frac{t}{\varepsilon}))\sin(\theta), \tag{1.1}$$

with initial conditions $\theta(0) = \theta_0, \dot{\theta}(0) = \omega_0$. When $1/\varepsilon$ is sufficiently large, and θ_0 and ω_0 are sufficiently close to 0, the pendulum will oscillate slowly back and forth with displacement $\theta < \theta_{\max}$. The period of the oscillation is "independent" of the forcing frequency ε, and in addition to this slow motion, the trajectory of θ also exhibits fast oscillations with amplitude and period proportional to ε. The behavior of this system and other generalizations are analyzed analytically in [9]. In short, the governing second order equation for these stiff problems take the general form

$$\ddot{x} = \varepsilon^{-1}a(\frac{t}{\varepsilon})f(x), \quad x(0) = x_0, \dot{x}(0) = y_0; \tag{1.2}$$

where a is a smooth, 1-periodic function, $0 < \varepsilon \ll 1$, and f is a bounded smooth function. It will be convenient to consider Eq.(1.2) as a system of first-order equations where $dx/dt = y$ and $dy/dt = \varepsilon^{-1}a(t/\varepsilon)f(x)$.

Typically, the computational difficulties in solving the above system stem from the eigenvalues of the Jacobian that have imaginary parts proportional to $\varepsilon^{-1/2}$ and from the short wavelength in the periodic function $a(t/\varepsilon)$. If explicit time stepping methods are employed to solve such a system, the corresponding stability condition requires the step size Δt to be

The second author is supported by NSF Grant No. DMS-0111298.

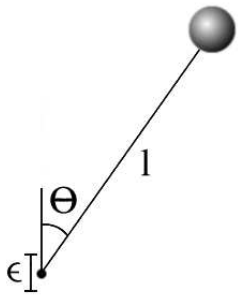

FIGURE 1.1. The inverted pendulum. A mass is connected to an arm of length l which makes an angle θ with the vertical axes.

proportional to $\varepsilon^{1/2}$, and if the solution is needed in an interval with length independent of ε, the computation would require $O(\varepsilon^{-1/2})$ operations, rendering the solution method unusable if ε is very small. On the other hand, implicit schemes with larger time steps typically damp out the oscillations or represent them inaccurately. There is also the problem of inverting the corresponding nonlinear system.

In many situations, one is interested in a set of quantities X that are derived from the solution of the given stiff system. Typically, these quantities change slowly in time. A pedagogical example, pointed out to the authors by G. Dahlquist, is the drift path of a mechanical alarm clock due to its shaking and rattling when it is set off on a hard surface. If the slowly changing quantities X depend only locally in time on the fast oscillations, it is then reasonable to devise a scheme that tracks the slow quantities by measuring the effects of the fast solutions only locally in time. Herein lies the possibility of reducing the computational complexity. Under this context, and recasting Eq.(1.2) as a first-order system, it is natural to look for an explicit numerical method that appears in the general form:

$$X_{n+1} = Q_H(\tilde{F}[x_n(t)], X_n, X_{n-1}, \cdots) \quad X_0 = X(0), \tag{1.3}$$

where $H = t^{n+1} - t^n$ denotes the slow time scale step size, h denotes the fast time scale step size, $x_n(t)$ is the microscopic data, and Q_H and $\tilde{F}$ denote some suitable operators; we will make precise all of these in the following. The functional $\tilde{F}$ relates x, the solution to the stiff problem, to the slowly changing quantities X.

In our specific problem with model (1.2), $x(t)$ is $\theta(t)$, and $X(t)$ is the average over the period $[t-\varepsilon/2, t+\varepsilon/2]$, $X(t) = \langle x \rangle = \frac{1}{\varepsilon}\int_{t-\varepsilon/2}^{t+\varepsilon/2} x(s/\varepsilon)ds$, and as shown in [9], it satisfies the averaged effective equation

$$\ddot{X} = \langle a \rangle f(X) - \left\langle v^2 \right\rangle f(X) f'(X) + E, \quad X(0) = X_0. \tag{1.4}$$

The "velocity", v is a function of the "acceleration" a,

$$v = \int_{s_0}^{t} \left(a(\frac{s}{\varepsilon}) - \langle a \rangle \right) ds \tag{1.5}$$

and s_0 is selected so that $\langle v \rangle = 0$. The error in Eq(1.4) is small, $|E| \sim O\left(\sqrt{\varepsilon}\right)$[9].

In fact, many existing methods can be cast into the above form (Eqs.(1.3,1.4)), with X directly related to either the strong or weak limit of the original variable x. For example, in the methods proposed in [5] and [10] for oscillatory ODEs, X is the envelope of x. The given stiff system from current state X_n for some integer number of periods $\eta = C\varepsilon$ fully resolving the oscillation with step size h. The method then estimates and returns the time derivative of the envelop, and finally Q_H corresponds to the discrete solution operator of the macroscopic scheme.

In [1], the general framework of Heterogeneous Multiscale Methods (HMM) was proposed. Under this framework approximation schemes can be more conveniently constructed and analyzed for general problems involving multiple separated temporal and spatial scales. In [3], under the HMM framework, we proposed and analyzed a class of HMM ODE schemes that operate in two time scales. There, the operator $\tilde{F}$ plays the role of approximating the average force by time filtering the microscopic evolution in the time interval $[t_n-\eta/2, t_n+\eta/2]$, using convolution with a suitable kernel. If the forward Euler scheme is adopted in Q_H, then the schemes appear to be

$$X_{n+1} = (X_n + H\cdot \tilde{F}[x_n(t)]).$$

The equations considered [3] in are of the form

$$\begin{cases} \frac{d}{dt}x = A(\frac{t}{\varepsilon})x + f(x,y) \\ \frac{d}{dt}y = g(x,y) \end{cases}.$$

It is proved there that if f does not depend on the phase of x, the constructed approximations converges to the solution of the averaged equation, and the averaged equation is of the following form:

$$\begin{cases} \frac{d}{dt}\bar{x} &= \frac{1}{2\pi}\int_0^{2\pi} e^{-i\phi} f(e^{i\theta}\bar{x},\bar{y})d\phi \\ \frac{d}{dt}\bar{y} &= \frac{1}{2\pi}\int_0^{2\pi} g(e^{i\phi}\bar{x},\bar{y})d\phi \end{cases}.$$

The class of second order equations under consideration in this paper, *i.e.* Equation (1.2), written as first order systems, do not fall into the category considered in [3]. However, it turns out that with some modifications to the schemes developed in [3], we can show that the modified HMM schemes approximate the averaged equations analyzed in [9]. This is the main purpose of our paper.

There has been much development of methods for special Hamiltonian systems $H(p,q) = \frac{1}{2}p^T M^{-1} p + W(q)$. These methods typically either assume an explicit separate grouping of solution components that change rapidly (fast modes) from the slow modes, or they assume that the potential W is the sum of a strong one and a weak one. Correspondingly, in the first case, slow and fast modes are solved separately in the whole interval $[t_n, t_n+H]$, and in the second case, a splitting approach is adopted to solve alternately the whole system with only the strong potential or the weak potential. They are called multirate methods and impulse method respectively. Please refer to [4], [6], [8], and more generally [7] for details. Even though these types of methods also use time averaging and appear to share certain resemblance to the HMM methods, it is important to point out that there is a fundamental difference. In the multirate or the impulse methods, the stiff part of the system, being either the fast modes or the split equations with strong potentials, is really solved globally in time, thus the high computational cost that results from the stiffness still remains. Whereas in the HMM methods, as we alluded earlier, the stiff system is solved only rarely for very short period of time. The macroscopic step size H is independent of ε and the overall number of operations is lower than ε^{-1}.

For a given $\varepsilon > 0$, all well known methods will converge as the step-size $H \to 0$, and there is no difference between stiff and nonstiff problems. We define what we mean by convergence such that it makes sense for very stiff problems ($\varepsilon \ll H$) by the following error:

$$E = \max_n(\lim_{H\to 0}(\sup_{0<\varepsilon<\varepsilon_0(H)} |X(t_n) - X_n|)). \tag{1.6}$$

Here, $\varepsilon_0(H)$ is a positive function of H, serving as an upper bound for the range of ε that we consider. With this notion, it is clear that a sensible multiscale method has to utilize the slow varying property of X and generate accurate approximation with a complexity sublinear to ε^{-1}.

The structure of the paper is as follows. In Section 2, we describe the HMM strategies of [1] in the context of building ODE schemes for problems with different time scales. In Section 3, we apply these types of schemes to compute average trajectories of an inverted pendulum. We then show in Section 4 the convergence of this scheme that is suggested by our numerical study. Finally, we summarize our results in Section 5.

2. HMM STRATEGY

A generic HMM method is described by the scheme used to evolve a system, denoted here by U, at macroscopic level, its accompanying microscopic scheme for the evaluation of the missing data, and the data transfer between the macro and micro systems. This missing data is here the effective force $\bar{f} = \langle f_\varepsilon \rangle$, see Eq.(2.1). A microscopic evolution of the system is invoked *only when* the effective force at certain time, t_n, is needed by the macro-scheme. At that time, the original equation

$$\frac{d}{dt}u = f_\varepsilon(u,t) \tag{2.1}$$

is solved accurately on the corresponding micro-grid, with the initial condition determined by RU, for a duration of time, η, to resolve the transient or the oscillations. The resulting microscale data, including the time history of microscale variables and the force, is then averaged by a suitable kernel K to evaluate the effective force and, in some cases, also a modified macroscopic variable U, at the appropriate time. We will use $\mathbb{K}^{p,q}$ to denote the kernel space discussed in this paper. $K \in \mathbb{K}^{p,q}(I)$ if $K \in C_c^q(\mathbb{R})$ with $\mathrm{supp}(K) = I$, and

$$\int_{\mathbb{R}} K(t)t^r dt = \begin{cases} 1, & r = 0; \\ 0, & 1 \le r \le p. \end{cases}$$

Furthermore, we will use $K_\eta(t)$ to denote the scaling of K: $K_\eta(t) := \eta^{-1}K(t/\eta)$.

Hence we may present the above procedures algorithmically as follows:

(1) Force estimation:
  (a) Reconstruction: at $T = t_n$, $R(U_n) \mapsto u_n$.
  (b) Solve for the micro variables: $u_n(t)$, for $t \in [t_n - \frac{\eta}{2}, t_n + \frac{\eta}{2}]$, with $u_n(t_n) = u_n$.
  (c) Compression: $U_* = Q[u_n]$.
  (d) Estimate force: $\bar{f}(t_*) = \bar{F}[u_n] = K_\eta * u_n(t_*)$.
(2) Evolve the macro variables: $\{U_n\} \bigcup \{U_*\} \longrightarrow U_{n+1}$, $T = t_{n+1}$.
(3) Repeat

The reconstruction operator and the compression operator should satisfy a compatibility condition:

$$Q(R(U)) = U.$$

An essential feature in this paper is the introduction of a reconstruction operator R so that the average of the fast modes in u is preserved in each microscopic evolution, and correspondingly, the compression operator Q that prepares the macroscopic variable in the suitable form.

We also notice that the number of micro-time steps needed depends on the nature of the problem. For example, for stiff problems with fast transients, we only need to evolve the micro variables until the transients vanish; in molecular dynamics, e.g. [2], the micro variables are evolved until equilibrium and then some further time to estimate the effective flux. We shall see that it also depends on the method used to estimate the effective force.

Figure 2.1 depicts schematics of the HMM ODE solvers. In these images, the top axis represents the macro grid used, and the bottom axis contains the microgrids established in a neighborhood of each macrogrid for microscale simulations. The arrow pointing from each macro grid point down to a micro grid denotes the action taken in step 1a, while the arrows pointing from each micro grid up toward the macro axis represent steps 1c and 1d.

The effective force is estimated either at some new time t_* which is laid down to be a new macroscale grid point, or the original macroscale grid point t_n, depending on the macroscale scheme used (see Figure 2.1). The advantage of schemes depicted in Figure 2.1 is that $\bar{f}$ can be evaluated on a uniform grid, and thus facilitate the implementation of linear multistep methods on the macro-grid. In the upper image in Figure 2.1, a non-symmetric kernel is needed to perform the force evaluation, and in the problems with transients, the macrogrid variables are projected to the invariant manifolds. The lower scheme in Figure 2.1 can be applied to reversible systems that have no transients. The advantage is the possibility of using symmetric kernels in force estimation.

We will call a method HMMpq-X-y, if X-method is used in step 2, y-method is used in Step 1b, and a kernel $K^{p,q}$ is used in Step 1d. Most of the time, we will suppress the parameters pq. Therefore, HMM-FE-rk4 is a method that uses forward Euler for macroscale evolution, and a fourth order Runge-Kutta method for microscale integrator. In Section 3, we will present a few standard HMM schemes and their stability in more detail. We only point out here that if X is a linear multistep method that requires uniform step size, then depending on the nature of the solutions, the structure of the HMM-X-* schemes are illustrated by Figure 2.1.

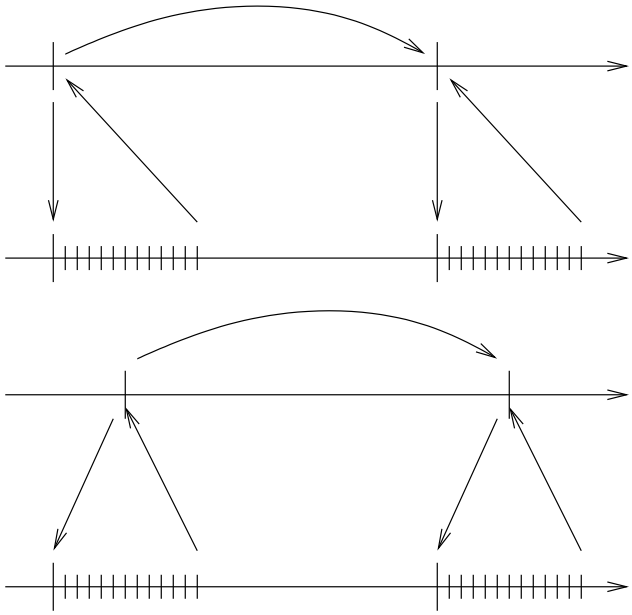

FIGURE 2.1. Schematic pictures of the interaction between the macro (upper lines) and micro (lower lines) scale computational domains for use with non-symmetric (top) and symmetric (bottom) kernels.

3. MAIN EXAMPLE

In this section, we propose three HMM ODE schemes to solve for the slow periodic motion of the inverted pendulum. Recall the original equation of motion for the pendulum,

$$l\ddot{\theta} = (g + \frac{1}{\varepsilon}\sin(2\pi\frac{t}{\varepsilon}))\sin\theta, \tag{3.1}$$

where θ is the angle between the pendulum and the upward vertical position, l is the length of the pendulum, and g is the gravitational constant. We will compare our approximations to the solution of the averaged equation,

$$l\ddot{\Theta} = g\sin\Theta - \frac{1}{8\pi^2 l}\sin\Theta\cos\Theta, \tag{3.2}$$

where $\Theta = \langle\theta\rangle$.

In this case the inverted pendulum could reach a maximum angle $\theta_{\max} = \cos^{-1}(gl/\langle v^2\rangle)$, subject to the stability criterion $gl < \langle v^2\rangle$. In the examples below $g = 0.1$ and $l = 0.05$ making $\theta_{\max} \approx 1.16$, although under the initial conditions $\theta_0 = 0, \quad \dot\theta_0 = -0.4$, the pendulum will sweep out a more conservative angle $\theta_\delta \approx 0.23$.

We use $u_n(t) = (\theta_n(t), \omega_n(t))$ to denote the solution of the first order system corresponding to equation (3.1), for $|t - t_n| \le \eta/2$ with $u_n(t_n) = (\theta_n(t_n), \omega_n(t_n))$ given. The function $\theta_n(t)$ represents the angle, and $\omega_n(t) = \dot\theta_n(t)$ is the angular velocity. Similarly, $U(t) = (\Theta(t), \Omega(t))$ denotes the solution to the averaged equation Eq.(3.2) for $t \ge t_0$ with $U(t_0) = (\Theta(t_0), \Omega(t_0))$ given, and $\Omega(t) = \dot\Theta(t)$. Discretize the averaged equation with time-step size H, $t_n = t_0 + nH, \quad n = 1, 2, 3, \ldots$ and $U_n = U(t_n)$.

Assume that the HMM strategy described in the previous section does discretize the average equation (3.2) by solving (3.1) locally near every t_n. This assumption imposes a compatibility condition on the reconstruction step; that is, if we set $u_n = (\theta_n, \omega_n) = R(U_n)$, then the force estimator should yield an approximation to the force of the averaged equation,

$$\tilde F[u_n(\cdot)] = \begin{pmatrix} \tilde F_{(1)}[u_n(\cdot)] \\ \tilde F_{(2)}[u_n(\cdot)] \end{pmatrix} = \begin{pmatrix} \Omega_n \\ g\sin\Theta_n - \frac{1}{(8\pi^2)l}\sin\Theta_n\cos\Theta_n \end{pmatrix}. \tag{3.3}$$

It is shown that $|\Theta(t) - \theta(t)| \sim O(\varepsilon)$ for $t \in (t_0, T]$ in [9], so taking $\theta_n = \Theta_n$ insures that $\Theta_n \approx \langle\theta_n(t)\rangle$. Writing Ω_n as the force acting on Θ at t_n gives,

$$\Omega_n = \omega_n + \left\langle \int_{t_n}^{t} a(\frac{s}{\varepsilon})\sin(\theta(s))ds \right\rangle.$$

Hence, we can set,

$$\begin{aligned} \omega_n &= \Omega_n - \left\langle \int_{t_n}^{t} a(\frac{s}{\varepsilon}) f(\theta_n(s))ds \right\rangle \\ &\approx \Omega_n - \sin(\Theta_n)\frac{\cos(2\pi\frac{t_n}{\varepsilon})}{2\pi l}, \end{aligned}$$

(in the second step we note that $\sin(\theta(s))$ varies slowly where $s \in [t_n - \varepsilon/2, t_n + \varepsilon/2]$) to ensure $\Omega_n \approx \langle\omega_n(t)\rangle$. Given a kernel $K \in \mathbb{K}^{p,q}$ as described in the previous section, let

$$\tilde F[u_n(\cdot)] = \begin{pmatrix} K * \omega_n(\cdot) \\ K * (g + \frac{1}{\varepsilon}\sin(2\pi\frac{(\cdot)}{\varepsilon}))\sin(\theta(\cdot)) \end{pmatrix}, \tag{3.4}$$

with initial conditions,

$$u_n = \begin{pmatrix} \Theta_n \\ \Omega_n - \sin\Theta_n\frac{\cos(2\pi t_n/\varepsilon)}{2\pi l} \end{pmatrix}.$$

The convolution $K * g(\cdot)$ is defined as

$$(K * f)(t) = \int_{t_n - \frac{\eta}{2}}^{t_n + \frac{\eta}{2}} K_\eta(t - s)g(s)ds,$$

where $K_\eta(t) = \frac{1}{\eta}K(\frac{t}{\eta})$. Using this estimated force, it will be possible to prove (in Section 4) that $\tilde F[u_n(\cdot)]$ approximates (3.3).

We present three HMM schemes and related numerical results for the inverted pendulum. The first order macroscopic Forward Euler schemes HMM-FE-* can be presented as follows:

Algorithm 3.1. *HMM-FE-**

Given $U_0 = (\Theta_0, \Omega_0)$, *for* $n = 0, 1, 2, ...$

$$\begin{aligned} \Theta_{n+1} &= \Theta_n + H \cdot \tilde{F}_{(1)}[\omega_n(\cdot)], \\ \Omega_{n+1} &= \Omega_n + H \cdot \tilde{F}_{(2)}[\theta_n(\cdot)], \end{aligned}$$

where $\tilde{F}[u_n(\cdot)]$ *is as defined by Eq(3.4).*

Provided that Y_n is sufficiently accurate, one may directly replace $\tilde{F}_{(1)}[u_n(\cdot)]$ with Ω_n. This is done in practice to reduce computation, and in this case there is no explicit need to calculate ω_n.

Next, a semi-implicit first order HMM-IFE-* scheme is,

Algorithm 3.2. *HMM-IFE-**

Given $U_0 = (\Theta_0, \Omega_0)$, for $n = 0, 1, 2, ...$

$$\begin{aligned} \Omega_{n+1} &= \Omega_n + H \cdot \tilde{F}_{(2)}[\theta_n(\cdot)] \\ \Theta_{n+1} &= \Theta_n + H \cdot \Omega_{n+1} \end{aligned}$$

In this case Ω_{n+1} is found using the explicit forward Euler step and then used to find Θ_{n+1}.

The final algorithm is a second order HMM-Verlet-* scheme is,

Algorithm 3.3. *HMM-Verlet-**

Given $U_n = (\Theta_n, \Omega_n)$, *for* $n = 0, 1, 2, ...$

$$\begin{aligned} \Omega_{n+\frac{1}{2}} &= \Omega_n + \frac{H}{2} \cdot \tilde{F}[\theta_n(\cdot)], \\ \Theta_{n+1} &= \Theta_n + H \cdot \Omega_{n+\frac{1}{2}}, \\ \Omega_{n+1} &= \Omega_{n+\frac{1}{2}} + \frac{H}{2} \cdot \tilde{F}[\theta_{n+1}(\cdot)], \end{aligned}$$

where $\theta_{n+1} = \Theta_{n+1}$ *is used to initialize the final force estimation.*

This final method requires twice the computational effort per macroscale step as the first order schemes, but the number of operations still much smaller than that of a direct calculation ($\eta/\varepsilon \ll T/\varepsilon$).

Several numerical simulations were completed using the parameters in Table 1.

TABLE 1. The parameters used for the numerical examples include ε, the initial condition (Θ_0, Ω_0), the time interval from t_0 to t_f, H (intervals indicate the range of values used for separate calculations to determine error behavior), h and η (both fixed and scaled with respect to H; r, s, p, and q in row three are the orders of the macroscale and microscale schemes, and the number of vanishing moments and smoothness of the kernel respectively, and α_h and α_η are constants), the exponential kernel K described in equation (3.5), the gravitational acceleration g, and the length of the pendulum arm l.

ε	(Θ_0, Ω_0)	$[t_0, T]$	H	η	h	K	g	l
10^{-6}	$(0.0, -0.4)$	$[0.0, 50.0]$	0.01	10ε	$\varepsilon/10$	exp	0.1	0.05
10^{-6}	$(0.0, -0.4)$	$[0.0, 12.0]$	$[0.001, 1.0]$	50ε	$\varepsilon/50$	exp	0.1	0.05
10^{-6}	$(0.0, -0.4)$	$[0.0, 12.0]$	$[0.001, 1.0]$	$\alpha_\eta H^{-s/q} \varepsilon^{1-1/q}$	$\alpha_h H^{s/r} \varepsilon^{1+2/r} \eta^{-1/r}$	exp	0.1	0.05

In each calculation, either the standard Verlet method (v) or fourth order Runge-Kutta (rk4) was used to solve the microscopic equations. In all cases, the exponential kernel

$$K = \frac{422.11}{\eta} \exp\left[5\left(\frac{4(t-t_n)^2}{\eta^2} - 1\right)^{-1}\right], \tag{3.5}$$

is used ($K \in \mathbb{K}^{1,\infty}$).

Figure 3.1 shows the macroscale behavior of the system over the period from $t_0 = 0$ to $T = 50$. The parameters used in the calculations are in the first row of Table 1. The HMM schemes HMM-FE-v and HMM-IFE-v are compared to the solution of the averaged equation (1.4). At the microscale, the resolution gives about 10 grid points per oscillation, and the convolution with K is a domain containing about 10 cycles. This is relatively coarse compared to later calculations. The computational savings, measured by the number of times the force is evaluated and compared to a traditional first order method using the same step-size h, is on the order of 10^9. More importantly, traditional methods cannot maintain sufficient accuracy to carry the calculation to $T = 50$.

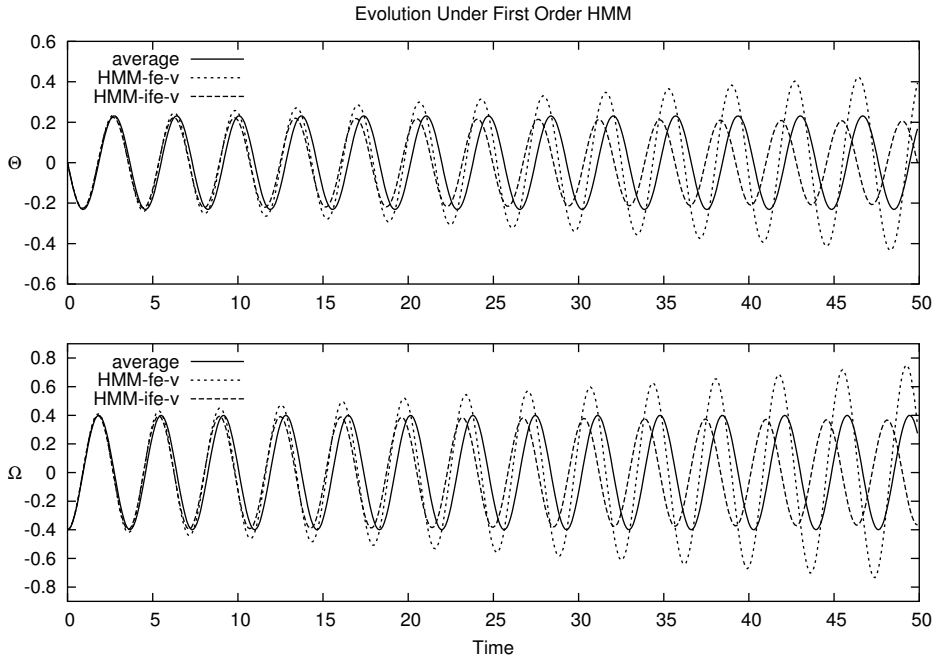

FIGURE 3.1. The HMM solution to equation (1.1); the top graph plots the angle $\Theta(t)$ and the lower graph gives $\Omega(t)$. In this case the first order methods HMM-FE-v and HMM-IFE-v were used to approximate the average motion of the pendulum over a long time interval. The solution of the averaged equation (1.4) is also shown for comparison. The parameters used to produce the graph are those in the first row of Table 1. Six orders of magnitude separate the period of the slow oscillation apparent in the graphs from the fast oscillation at the microscale.

The force estimation error for HMM is $\mathcal{E}_{HMM} = \mathcal{E}_{\text{micro}} + \mathcal{E}_K + \mathcal{E}_{\text{quad}}$ and the local error of the HMM scheme is

$$\mathcal{E}_n = \mathcal{E}_H + \mathcal{E}_{HMM}.$$

$\mathcal{E}_H$ denotes the local truncation error of the macroscopic scheme, and in many cases, $\mathcal{E}_H$ dominates and determines the order of $\mathcal{E}_n$. The convergence of various HMM schemes as

$H \to 0$ was confirmed using the error metric,

$$E = \max_n \sqrt{(\Theta_n - \Theta(t_n))^2 + (\Omega_n - \Omega(t_n))^2} \tag{3.6}$$

where $\Theta(t)$ and $\Omega(t)$ are values of the solution of the averaged equation. Error calculations were carried out over the time period $[0,12]$, corresponding to roughly three oscillations on the macroscale. Figure 3.2 shows error as a function of $1/H$ for the first order methods HMM-FE-* and HMM-IFE-*. The calculations correspond to row two of Table 1. In all cases η and h are fixed with respect to H, and $O(H)$ convergence is achieved. In the HMM-IFE-v method however, approximation error associated with the microscale calculation and convolution dominates the contribution from $\mathcal{E}_H$, for small H.

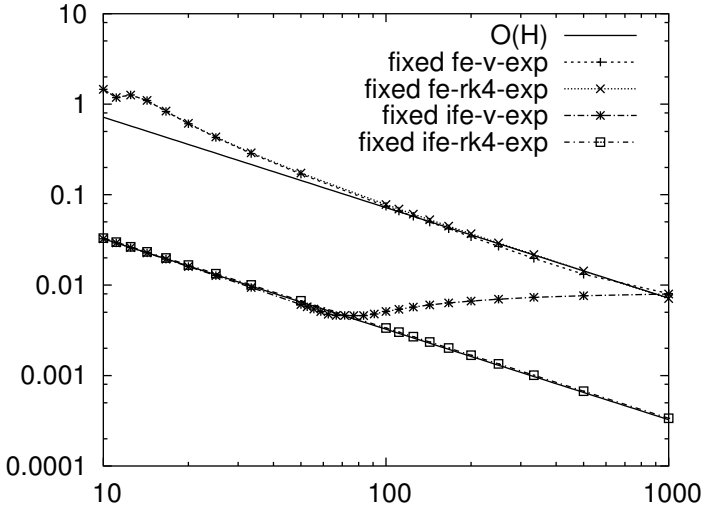

FIGURE 3.2. The error as a function of $1/H$ for the first order schemes HMM-X-y, where X is FE or IFE and y is v or rk4. The width of the microscale domain and the step-size h are fixed with respect to H. The parameters used are listed in row two of Table 1. The slopes of the solid lines indicate decrease at first order in H.

Figure 3.3 shows the analogous cases for the second order methods HMM-V-*. As previously, the HMM-X-v method levels off due to other contributions to the overall error, while HMM-X-rk4 is able to maintain its performance for small H.

Notice that some of the curves in Figures 3.2 and 3.3 eventually flattens out as $1/H$ increases. These are the situations in which the error $\mathcal{E}_{HMM}$ finally dominates the global error of the computations. It is possible to overcome the flattening of the HMM-X-v cases by scaling the parameters η and h with H. See [3] for more detail. By setting $\eta = \alpha_\eta H^{-s/q}\varepsilon^{1-1/q}$ and $h = \alpha_h H^{s/r}\varepsilon^{1+2/r}\eta^{-1/r}$, where r, s, p, and q are the orders of the macroscale and microscale schemes, and the number of vanishing moments and smoothness of the kernel respectively, and α_h and α_η are constants, the HMM-V-v scheme is able to maintain second order behavior as shown in Figure 3.4. The drawback to scaling is that the constants α_h and α_η need to be chosen carefully to place η and h in reasonable ranges.

HMM-V-rk4 maintains its second order performance as H decreases in the case of fixed η and h. This performance is matched when η and h are scaled as described above as shown in Figure 3.5.

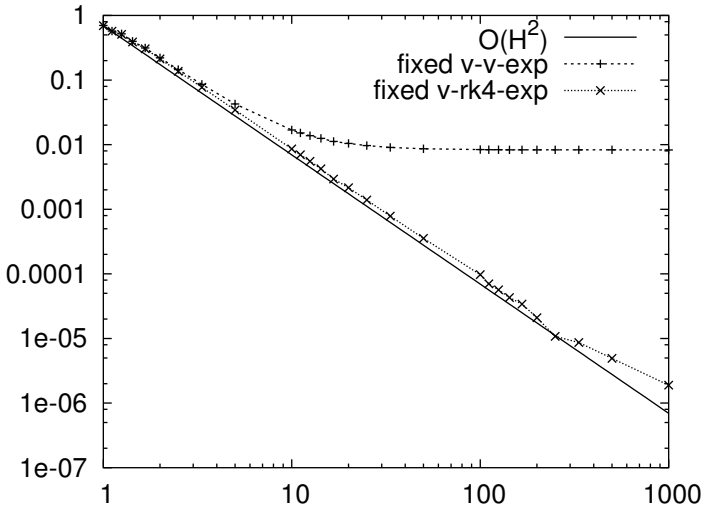

FIGURE 3.3. The error as a function of $1/H$ for the second order schemes HMM-V-y, where y is v or rk4. The width of the microscale domain and the step-size h are fixed with respect to H. The parameters used are listed in row two of Table 1. The slope of the solid line indicates decrease at second order in H.

4. GENERALIZATIONS

It is clear from the HMM structure that the stability of an HMM scheme requires that both the macroscopic and microscopic schemes to be stable. It remains to establish the consistency of the estimated force in Eq.(3.4). The notion of consistency can be defined as in (1.6). Consider the general case

$$\ddot{x} = a_\varepsilon(\frac{t}{\varepsilon}) f(x), \quad x(0) = x_0, \dot{x}(0) = y_0 \tag{4.1}$$

and the associated averaged equation

$$\ddot{X} \quad = \quad \langle a_\varepsilon \rangle f(X) - \langle v^2 \rangle f(X) f'(X) + C\sqrt{\varepsilon}. \tag{4.2}$$

The function $a_\varepsilon(t)$ is assumed to be smooth with $||a_\varepsilon||_\infty \sim O(\varepsilon^{-1})$, periodic with period 1, and $f \in C^p$ is assumed to vary slowly $||f^{(k)}||_\infty < C_0$ for $k = 0, \cdots, p$. It will be important to note that $\langle a_\varepsilon \rangle \sim O(1)$.

The basic assumption is that a_ε contains the fast periodic motion in the problem and f is relatively slow. These assumptions hold in the case of the inverted pendulum. In this case $a_\varepsilon = a_\varepsilon(t/\varepsilon)$, $||x|| \le x_{\max} \sim O(1)$, $f(x) \approx f(X)$, and $||x'|| \le E_y = \sqrt{2(E_0 - g)/l} \sim O(1)$. The constants $x_{\max}$ and E_0 are determined by the given parameters and initial conditions. They may be calculated by considering the effective potential, $V(x) = g\cos(x) + \sin^2 x/16\pi^2 l$ implied by Eq.(3.2), and the energy $E_0 = l y_0^2/2 + V(x_0)$.

In the discussion which follows we will make use of the velocity

$$v(\frac{s}{\varepsilon}) = \int_{s_n}^{s} (a_\varepsilon(\frac{\sigma}{\varepsilon}) - \langle a_\varepsilon \rangle) ds, \quad s \in [t_n - \frac{\eta}{2}, t_n + \frac{\eta}{2}]$$

where s_n is chosen so that $\langle v \rangle = 0$ and $|s_n - t_n| \le \varepsilon$. The velocity is related to x' and likewise the scaling of a_ε implies that $||v||_\infty \sim O(1)$. Another useful term will be $\Delta x = x(s) - X_n, \quad s \in [t_n - \eta/2, t_n + \eta/2]$. Provided that $||x'||_\infty$ is bounded as shown above, Δx is small.

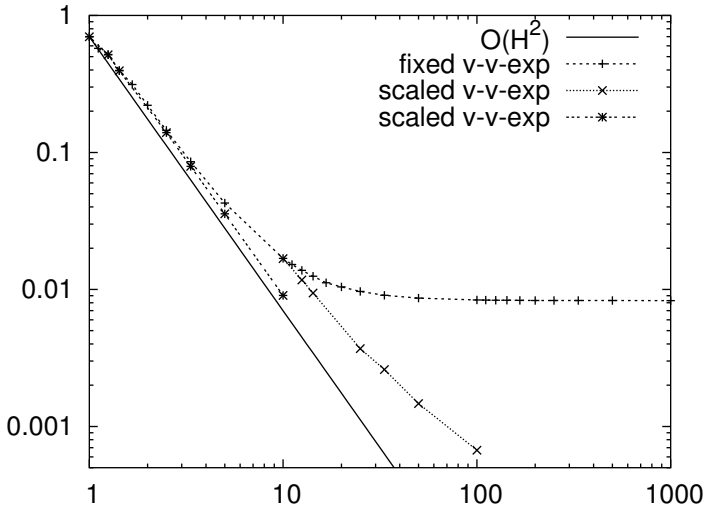

FIGURE 3.4. A comparison of the error, as a function of $1/H$, for the second order schemes HMM-V-v for fixed and scaled microscale domains and step-sizes. The parameters and scaling used are listed in rows two and three of Table 1. The slope of the solid line indicates decrease at second order in H. In the cases where η and h are scaled with respect to H, the method is able to maintain second order performance, despite the leveling off seen in the fixed case. The constants α_h and α_η were chosen such that the scaled and fixed versions of the calculation would match at $H = 0.1$ and $H = 1$. The constants were reset at these values of H so that the ratio of η to h would remain reasonable as H decreases.

Lemma 4.1. *(Δx is small) $\Delta x = x(s) - X_n$, for $s \in [t_n - \eta/2, t_n + \eta/2]$*

$$|\Delta x| \leq C_1\varepsilon + C_2\eta$$

Proof. >From [9] we have $|x(t_n) - X_n| \leq C\varepsilon$.

$$\begin{aligned} |x(s) - X_n| &\leq |x(t_n) - X_n| + |\int_{t_n}^{s} x'(\tau)d\tau| \\ &\leq C\varepsilon + \frac{\eta}{2}||x'||_\infty. \end{aligned}$$

□

A more explicit description of $x'(s)$ will also be needed in addition to its boundedness.

Lemma 4.2. *(Expression for $x'(s)$)*

$$x'(s) = f(X_n)v(\frac{s}{\varepsilon}) + x'(s_n) + f(X_n)\langle a\rangle(s - s_n) + \int_{s_n}^{s} a_\varepsilon(\frac{\sigma}{\varepsilon})f'(z)\Delta x d\sigma$$

Proof. By definition

$$\begin{aligned} x'(s) &= x'(s_n) + \int_{s_n}^{s} a_\varepsilon(\frac{\sigma}{\varepsilon})f(x(\sigma))d\sigma \\ &= x'(s_n) + f(X_n)\langle a_\varepsilon\rangle(s - s_n) + f(X_n)\int_{s_n}^{s}(a(\frac{\sigma}{\varepsilon}) - \langle a\rangle)d\sigma + \int_{s_n}^{s} a(\frac{\sigma}{\varepsilon})f'(z)\Delta x d\sigma \\ &= x'(s_n) + f(X_n)\langle a_\varepsilon\rangle(s - s_n) + f(X_n)v(\frac{s}{\varepsilon}) + \int_{s_n}^{s} a(\frac{\sigma}{\varepsilon})f'(z)\Delta x d\sigma \end{aligned}$$

□

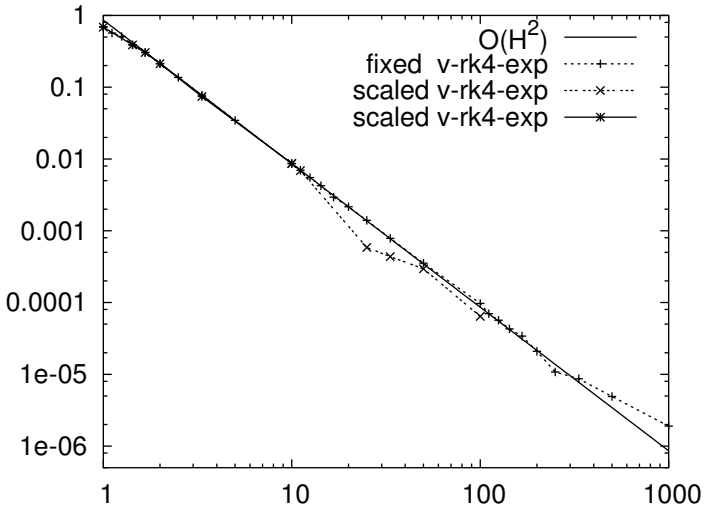

FIGURE 3.5. A comparison of the error, as a function of $\frac{1}{H}$, for the second order schemes HMM-V-rk4 for fixed and scaled microscale domains and step-sizes. The parameters and scaling used are listed in rows two and three of Table 1. The slope of the solid line indicates decrease at second order in H. In the case where η and h are scaled with respect to H, the method is able to match the second order performance of the fixed method.

In the previous section, the problem is recast as a first order system of equations, and the average force is estimated by using the microscale solution with suitable initial data. The force

$$\begin{pmatrix} \tilde{F}_{(1)} \\ \tilde{F}_{(2)} \end{pmatrix} = \begin{pmatrix} K*y \\ K*\ddot{x} \end{pmatrix},$$

given the initial data

$$\begin{pmatrix} x_n \\ y_n \end{pmatrix} = \begin{pmatrix} X_n \\ Y_n - f(X_n)\langle \int_{t_n}^{s} a_\varepsilon(\frac{\sigma}{\varepsilon})d\sigma \rangle \end{pmatrix},$$

accurately estimates the average force of Eq.(4.2). The accuracy of the force estimator $\tilde{F}_{(1)}$ may be quickly shown given the initial value y_n above.

Theorem 4.3. *(Consistency of $\tilde{F}_{(1)}$) Given $\tilde{F}_{(1)} = K*y$, $K \in \mathbb{K}^{p,q}$,*

$$|K*y - Y(t_n)| \leq C\frac{\eta}{\varepsilon}||\Delta x||_\infty$$

Proof. By definition,

$$\begin{aligned} K*y &= \int_{t_n-\frac{\eta}{2}}^{t_n+\frac{\eta}{2}} K_\eta(t-s)y(s)ds \\ &= \int_{t_n-\frac{\eta}{2}}^{t_n+\frac{\eta}{2}} K_\eta(t-s)(y_n + f(X_n)\int_{t_n}^{s} a_\varepsilon(\frac{\sigma}{\varepsilon})d\sigma + \int_{t_n}^{s} a_\varepsilon(\frac{\sigma}{\varepsilon})f(z)\Delta x d\sigma)ds \\ &= Y_n + O(\frac{\eta}{\varepsilon}||\Delta x||_\infty) \end{aligned}$$

□

We now prove our main result, that the force estimator $\tilde{F}_{(2)}$ provides a good approximation of the averaged force $\ddot{X}$.

Theorem 4.4. *(Consistency of $\tilde{F}_{(2)}$) Let $K \in \mathbb{K}^{p,q}$, $g(t) = a_\varepsilon(t/\varepsilon) f(x(t))$, then*

$$|K * g - \ddot{X}(t_n)| \leq O(||\Delta x||_\infty, \frac{||\Delta x||_\infty^2}{\varepsilon}, \frac{\varepsilon^{q-1}}{\eta^q}, \eta^p, \sqrt{\varepsilon})$$

Proof. Let $G(t) = \langle a_\varepsilon \rangle f(X) - \langle v^2 \rangle f(X) f'(X)$, we first show that $K * g \sim G$.

$$\begin{aligned} K * g &= \int_{t_n - \frac{\eta}{2}}^{t_n + \frac{\eta}{2}} K_\eta(t-s) a_\varepsilon(\frac{s}{\varepsilon}) f(x(s)) ds \\ &= f(X_n) \int_{t_n - \frac{\eta}{2}}^{t_n + \frac{\eta}{2}} K_\eta(t-s) a_\varepsilon(\frac{s}{\varepsilon}) ds + f'(X_n) \int_{t_n - \frac{\eta}{2}}^{t_n + \frac{\eta}{2}} K_\eta(t-s) a_\varepsilon(\frac{s}{\varepsilon}) \Delta x ds \\ &\quad + \int_{t_n - \frac{\eta}{2}}^{t_n + \frac{\eta}{2}} K_\eta(t-s) a_\varepsilon(\frac{s}{\varepsilon}) f''(z) \frac{\Delta x^2}{2} ds \\ &= I_1 + I_2 + I_3 \end{aligned}$$

Consider I_3,

$$\begin{aligned} |I_3| &\leq \frac{1}{2} ||a_\varepsilon||_\infty \cdot ||f''||_\infty \cdot ||\Delta x||_\infty^2 \int_{t_n - \frac{\eta}{2}}^{t_n + \frac{\eta}{2}} |K_\eta(t-s)| ds \\ &\sim O(||\Delta x||_\infty^2 / \varepsilon). \end{aligned}$$

In many cases (including the numerical examples in the previous section) the kernel will be a positive function, and $\int_{t_n - \frac{\eta}{2}}^{t_n + \frac{\eta}{2}} |K_\eta(t-s)| ds = 1$. Using the results in [3] we may estimate I_1,

$$\begin{aligned} I_1 &= \langle a_\varepsilon \rangle f(X_n) + f(X_n) \int_{t_n - \frac{\eta}{2}}^{t_n + \frac{\eta}{2}} K(t-s)(a_\varepsilon(\frac{s}{\varepsilon}) - \langle a_\varepsilon \rangle) ds \\ &\leq \langle a_\varepsilon \rangle f(X_n) + ||f||_\infty \cdot ||a_\varepsilon||_\infty \left(\frac{\varepsilon}{\eta} \right)^q \\ &\leq \langle a_\varepsilon \rangle f(X_n) + O\left(\frac{\varepsilon^{q-1}}{\eta^q} \right) \end{aligned}$$

The estimate of I_2 is slightly more involved,

$$\begin{aligned} I_2 &= \langle a_\varepsilon \rangle f'(X_n) \int_{t_n - \frac{\eta}{2}}^{t_n + \frac{\eta}{2}} K_\eta(t-s) \Delta x ds + f'(X_n) \int_{t_n - \frac{\eta}{2}}^{t_n + \frac{\eta}{2}} K_\eta(t-s)(a_\varepsilon(\frac{s}{\varepsilon}) - \langle a_\varepsilon \rangle) \Delta x ds \\ &= \langle a_\varepsilon \rangle f'(X_n) \int_{t_n - \frac{\eta}{2}}^{t_n + \frac{\eta}{2}} K_\eta(t-s) \Delta x ds + f'(X_n) \int_{t_n - \frac{\eta}{2}}^{t_n + \frac{\eta}{2}} K'_\eta(t-s) v(\frac{s}{\varepsilon}) \Delta x ds \\ &\quad - f'(X_n) \int_{t_n - \frac{\eta}{2}}^{t_n + \frac{\eta}{2}} K_\eta(t-s) v(\frac{s}{\varepsilon}) x'(s) ds \end{aligned}$$

where $v(s/\varepsilon) = \int_{s_0}^{s} (a_\varepsilon(\sigma/\varepsilon) - \langle a_\varepsilon \rangle) d\sigma$, and $\langle v \rangle = 0$.

Using the previous estimate for $x'(s)$

$$\begin{aligned} I_2 &= f'(X_n)\langle a_\varepsilon\rangle \int_{t_n-\frac{\eta}{2}}^{t_n+\frac{\eta}{2}} K_\eta(t-s)\Delta x ds + f'(X_n)\int_{t_n-\frac{\eta}{2}}^{t_n+\frac{\eta}{2}} K'_\eta(t-s)v(\frac{s}{\varepsilon})\Delta x ds \\ &\quad - f'(X_n)f(X_n)\langle v^2\rangle - (f'(X_n)f(X_n)\int_{t_n-\frac{\eta}{2}}^{t_n+\frac{\eta}{2}} K_\eta(t-s)(v^2(\frac{s}{\varepsilon}) - \langle v^2\rangle)ds \\ &\quad + f'(X_n)x'(s_0)\int_{t_n-\frac{\eta}{2}}^{t_n+\frac{\eta}{2}} K_\eta(t-s)v(\frac{s}{\varepsilon})ds \\ &\quad + f'(X_n)f(X_n)\langle a_\varepsilon\rangle \int_{t_n-\frac{\eta}{2}}^{t_n+\frac{\eta}{2}} K_\eta(t-s)v(\frac{s}{\varepsilon})(s-s_0)ds \\ &\quad + f'(X_n)\int_{t_n-\frac{\eta}{2}}^{t_n+\frac{\eta}{2}} K_\eta(t-s)v(\frac{s}{\varepsilon})\int_{s_0}^{s} a_\varepsilon(\frac{\sigma}{\varepsilon})f'(z)\Delta x d\sigma ds) \\ &= -f'(X_n)f(X_n)\langle v^2\rangle + O(||\Delta x||_\infty, \left(\frac{\varepsilon}{\eta}\right)^q, \eta^p) \end{aligned}$$

Combining these results yields the complete estimate,

$$\begin{aligned} |K*g - \ddot{X}(t_n)| &= |K*g - G + C\sqrt{\varepsilon}| \\ &\sim O(||\Delta x||_\infty, \frac{||\Delta x||_\infty^2}{\varepsilon}, \frac{\varepsilon^{q-1}}{\eta^q}, \eta^p, \sqrt{\varepsilon}). \end{aligned}$$

□

5. Conclusion

The inverted pendulum exhibits stable slow oscillation due to rapid microscale oscillatory forcing. This macroscale behavior is captured very well by a set of HMM algorithms for which the computational complexity is much lower than that of standard numerical methods. The HMM approach requires only $O(T/H\cdot\eta/\varepsilon)$ operations, which lead to a computational savings of $O(\eta/H)$ or about 10^3 for the parameters in our numerical experiments compared to standard numerical methods. Notably, standard methods lack sufficient accuracy to solve the model problem here with $\varepsilon = 10^{-6}$ for macroscopic time scales.

References

[1] Weinan E and Bjorn Engquist. The heterogeneous multiscale methods. *Comm. Math. Sci.*, 1(1):87–132, 2003.

[2] Weinan E and Xiantao Li. Heterogeneous multiscle method for phase transitions. *In Preparation*.

[3] Bjorn Engquist and Yen-Hsi Tsai. Heterogeneous multiscale methods for stiff ordinary differential equations. 2003. Under review.

[4] B. García-Archilla, J. M. Sanz-Serna, and R. D. Skeel. Long-time-step methods for oscillatory differential equations. *SIAM J. Sci. Comput.*, 20(3):930–963 (electronic), 1999.

[5] C. W. Gear and K. A. Gallivan. Automatic methods for highly oscillatory ordinary differential equations. In *Numerical analysis (Dundee, 1981)*, volume 912 of *Lecture Notes in Math.*, pages 115–124. Springer, Berlin, 1982.

[6] C. W. Gear and D. R. Wells. Multirate linear multistep methods. *BIT*, 24(4):484–502, 1984.

[7] Ernst Hairer, Christian Lubich, and Gerhard Wanner. *Geometric numerical integration*, volume 31 of *Springer Series in Computational Mathematics*. Springer-Verlag, Berlin, 2002. Structure-preserving algorithms for ordinary differential equations.

[8] Ben Leimkuhler and Sebastian Reich. A reversible averaging integrator for multiple time-scale dynamics. *J. Comput. Phys.*, 171(1):95–114, 2001.

[9] Mark Levi. Geometry and physics of averaging with applications. *Phys. D*, 132(1-2):150–164, 1999.

[10] Linda R. Petzold. An efficient numerical method for highly oscillatory ordinary differential equations. *SIAM J. Numer. Anal.*, 18(3):455–479, 1981.

PROGRAM IN APPLIED AND COMPUTATIONAL MATHEMATICS, PRINCETON UNIVERSITY, FINE HALL, WASHINGTON ROAD, NJ 08544
E-mail address: rsharp@math.princeton.edu

INSTITUTE FOR ADVANCED STUDY, AND DEPARTMENT OF MATHEMATICS PRINCETON UNIVERSITY, FINE HALL, WASHINGTON ROAD, NJ 08544
E-mail address: ytsai@math.princeton.edu

DEPARTMENT OF MATHEMATICS AND PACM, PRINCETON UNIVERSITY, FINE HALL, WASHINGTON ROAD, NJ 08544